THE ASTROPHYSICAL JOURNAL, 443:18–28, 1995 April 10

ON THE UNIVERSALITY OF MICROLENSING IN QUADRUPLE GRAVITATIONAL LENSES

HANS J. WITT,[1] SHUDE MAO,[2] AND PAUL L. SCHECHTER[3]
Received 1994 July 5; accepted 1994 October 19

ABSTRACT

It is well known that mutiply imaged quasars are likely to be affected by microlensing. Quadruply imaged systems are especially useful laboratories for studying microlensing because their macrolens models are relatively well constrained. We begin with analytical results for a simple family of galaxy models. These results can be used to estimate the magnifications and time delays for the quadruple systems. We compute expected brightness fluctuations due to microlensing in several such systems for a range of source sizes. Among these we treat for the first time the limiting case of a completely unresolved source.

For the case of MG 0414+0534 we interpret the discrepant optical-to-radio flux ratios for the different components as the result of microlensing. On the assumption that the lensing galaxy is roughly isothermal this gives a 95% confidence upper limit on the optical source size of 10^{16} cm $\times$ $(\langle M\rangle/0.1\ M_\odot)^{1/2}$ where $\langle M\rangle$ is the average stellar mass of the lensing galaxy. For more centrally concentrated macromodels the upper limit is greater. Sufficiently long strings of photometric observations can in principle constrain the degree of concentration.

Subject headings: gravitational lensing—quasars: general—quasars: individual (MG 0414+0534)

1. INTRODUCTION

Gravitational microlensing (Chang & Refsdal 1979; Young 1981; Gott 1981) has now been firmly established in the quadruple lens 2237+0305 (Irwin et al. 1989; Pen et al. 1993; Houde & Racine 1994, and references therein). Indications of microlensing have also been found in gravitational lenses 0957+561 (Schild & Smith 1991; Falco, Wambsganss, & Schneider 1991), and in the quadruple lenses PG 1115+080 (Vanderiest et al. 1986; Schechter 1995), H1415+117 (Altieri & Giraud 1991, Arnould et al. 1993) and MG 0414+0534 (Schechter & Moore 1993; Falco 1993; Angonin-Willaime et al. 1994). There have been numerous theoretical studies (e.g., Kayser, Refsdal, & Stabell 1986; Wambsganss & Paczyński 1991; Witt & Mao 1994, and references therein) of microlensing in such systems, most of which focus on 2237+0305 and were carried out prior to the observation of microlensing events in this system. While the quadruple lens 2237+0305 has the most favorable microlensing geometry of all known systems, there has been a widespread appreciation that microlensing should be a general property for multiply imaged quasars (Blandford & Narayan 1992; Refsdal & Surdej 1994). Nevertheless little quantitative theoretical work has been done on systems other than 2237+0305.

In this paper, we investigate macromodels for several known quadruple lenses (listed below) and use them to predict microlensing amplitudes and timescales. The theoretical models for these systems are better constrained than those for the two image systems. Moreover, the time delays between images are expected to be small, so that the microlensing events can be readily distinguished from the intrinsic variations. These systems are therefore particularly suitable for microlensing studies. In § 2, we illustrate the uncertainties in the theoretical modeling by analyzing a simple potential parameterization. In § 3, we perform microlensing calculations for models of known quadruple systems and estimate the optical variability of the quadruple images caused by microlensing and the timescales for microlensing. We compare our theoretical results with the observations of MG 0414+0534 to obtain a limit on the size of the quasar. In § 4, we summarize our results and draw conclusions.

2. MACROMODELS

Five confirmed quadruple lenses are listed in Table 2 below. The source redshifts are known for all the lenses. Plausible identifications of the lensing galaxy have been made for all except 1413+117 (see the table in Surdej et al. 1993, p. 207, and references therein). In two cases redshifts have been measured from absorption lines, and in a third, MG 0414+0534, a Na D line has been identified recently at redshift 0.468 (Lawrence, Cohen, & Oke 1995). All the lenses have been modeled theoretically. The image positions can be fitted with a precision $\lesssim 0\farcs02$ for some lenses (1115+080, 2237+0305, and 1413+117), while others are more difficult to fit. Furthermore the theoretical flux ratios are only consistent with the observed flux ratios within a factor of 2 (e.g., Kochanek 1991; Witt & Mao 1994; Wambsganss & Paczyński 1994; Hogg & Blandford 1994, Kormann, Schneider, & Bartelmann 1994). A variety of potential forms have been shown to fit the lenses equally well (Kochanek 1991; Wambsganss & Paczyński 1994). In this paper we will study a simple family of models similar to those used in Wambsganss & Paczyński (1995). The models are sufficiently simple to derive some general analytical results which we then use to investigate the essentials of macromodels.

[1] Princeton University Observatory, Peyton Hall, Princeton, NJ 08544.
[2] MS 51, Center for Astrophysics, 60 Garden Street, Cambridge, MA 02138.
[3] Department of Physics, Massachusetts Institute of Technology, Cambridge, MA 02139.

We adopt a two-dimensional potential ϕ with the following form

$$\phi(x, y) = \frac{b^{2-\beta}}{\beta} r^{\beta} + \frac{\gamma_g}{2}(x^2 - y^2), \qquad 0 < \beta < 2 \tag{1}$$

where $\boldsymbol{r} = (x, y)$ gives the angular coordinates on the deflector plane, b is the critical radius, β is the power-law index of the potential with respect to the radius r, and γ_g is a small global external shear to break the spherical symmetry of the potential. Since for $\gamma_g = 0$ the potential would yield only two images, a global shear is needed to obtain four images. Notice that since the potential is singular at the origin, we have either two or four images depending on whether the source lies outside outside or inside the central caustics. All the lengths in equation (1) are expressed in angular units. All of the following results can be extended to the case $\beta = 0$, the case of a point mass, for which the two-dimensional potential is proportional to $\ln r$.

For a given global shear term γ_g, one can show that for an image at radius r, the surface density κ and shear γ as defined by Young (1981) are given by

$$\kappa(r) = \frac{\beta}{2}\left(\frac{b}{r}\right)^{2-\beta}, \qquad \gamma(r) = \left\{\gamma_g^2 - \gamma_g(2-\beta)\left(\frac{b}{r}\right)^{2-\beta}\frac{x^2 - y^2}{r^2} + \left(\frac{b}{r}\right)^{4-2\beta}\frac{(2-\beta)^2}{4}\right\}^{1/2}. \tag{2}$$

As an example, for $\gamma_g = 0$, we have $\kappa = \gamma = \frac{1}{2}$ at the critical radius ($r = b$) for a singular isothermal sphere ($\beta = 1$). Note that the surface mass density and shear term at the position of a macroimage are the important quantities for studies of the microlensing behavior of the image. We will return to this point in § 3.

For the full potential in equation (1), the lens equations are

$$\xi = x - \frac{\partial\phi}{\partial x}, \qquad \text{and} \qquad \eta = y - \frac{\partial\phi}{\partial y}, \tag{3}$$

where ξ and η are the angular coordinates of the source. For the special cases $\beta = 0$ and $\beta = 1$ the lens equation can be simplified into a quartic equation and then solved analytically. If the source is placed on the ξ- or η-axis the problem can be further simplified to two quadratic equations. Here we solve the lens equation only for the case when the source is exactly aligned with the line of sight ($\xi = \eta = 0$). The four image positions are then, respectively,

$$x_{1,2} = 0, \qquad y_{1,2} = \pm\frac{b}{(1+\gamma_g)^{1/(2-\beta)}}, \qquad x_{3,4} = \pm\frac{b}{(1-\gamma_g)^{1/(2-\beta)}}, \qquad y_{3,4} = 0. \tag{4}$$

The surface densities, external shears (vector sums of the global and local shears) and magnifications are

$$\begin{aligned} \kappa_{1,2} &= \frac{\beta}{2}(1+\gamma_g), \quad \gamma_{1,2} = 1 - \frac{\beta}{2} + \left(2 - \frac{\beta}{2}\right)\gamma_g, \quad \mu_{1,2} = -\frac{1}{2\gamma_g(1+\gamma_g)(2-\beta)}, \\ \kappa_{3,4} &= \frac{\beta}{2}(1-\gamma_g), \quad \gamma_{3,4} = 1 - \frac{\beta}{2} - \left(2 - \frac{\beta}{2}\right)\gamma_g, \quad \mu_{3,4} = \frac{1}{2\gamma_g(1-\gamma_g)(2-\beta)}. \end{aligned} \tag{5}$$

The total magnification can then be found to be

$$\mu = \frac{2}{\gamma_g(1-\gamma_g^2)(2-\beta)}. \tag{6}$$

Notice that when β increases, the total magnification also increases. Another interesting quantity is the time delay between the images. Using the time delay map (see Schneider, Ehlers, & Falco 1992, 171):

$$\Delta t(x, y) = \frac{D}{c}(1+z_d)\left[\frac{(x-\xi)^2 + (y-\eta)^2}{2} - \phi(x, y)\right], \tag{7}$$

where z_d is the redshift of the lens, and $D = D_d/D_{ds}$ with D_d, D_s, and D_{ds} being the distance to the deflector, the distance to the source and the distance between the deflector and the source, we obtain the time by which the two images on the y-axis lag the two images on the x-axis when the source is at the origin,

$$\Delta t = (1+z_d)\frac{D}{c}b^2\frac{2-\beta}{2\beta}\left[(1+\gamma_g)^{-\beta/(\beta-2)} - (1-\gamma_g)^{-\beta/(2-\beta)}\right], \qquad 0 < \beta < 2 \tag{8}$$

Now let us apply our analysis to the observed systems. Kochanek (1991) showed that the critical radius b is extremely well constrained. After the models satisfy the critical radius constraint, the main constraint left is the axis ratio. That is, for models with different β, the axis ratio of the predicted images, $R = |(y_1 - y_2)/(x_3 - x_4)|$, must be the same as the observed axis ratio $R_{\rm obs}$. In the limit of small external shear γ_g this condition can be expressed as

$$\gamma_g \approx \frac{(2-\beta)(1-R)}{2}. \tag{9}$$

Substituting this condition into equations (6) and (8), we obtain the total magnification and time delay as a function of β

$$\mu \approx \frac{4}{(2-\beta)^2(1-R)}, \qquad \Delta t = (1+z_d)\frac{D}{c} b^2 \frac{(2-\beta)(1-R)}{2}. \tag{10}$$

The lensing galaxy in 2237+0305 is closely aligned with the line of sight. For 1413+117, the lensing galaxy is not yet detected, however the image configuration strongly suggests a nearly perfect alignment of the lens and the line of sight. Our analysis is therefore particularly appropriate for these two quadruple systems. We estimate the axis ratio by simply dividing the distances between the diagonal pairs of images. This gives $R \approx 0.90$ for 2237+0305, $R = 0.8$ for 1413+117. Substituting these values into equation (10), we obtain $\mu = 40$ for 2237+0305 and $\mu = 20$ for 1413+117, these values should be compared with the numerical results (reported below) $\mu = 30$ and $\mu = 18.5$. The larger difference of 2237+0305 is expected because this system is not as symmetric as 1413+117. All of the scalings are in excellent agreement with the results in Wambsganss & Paczyński (1995).

We now model the systems more realistically using the χ^2 minimization method of Kayser et al. (1990) and Kochanek (1991). For PG 1115+080 and 1413+117, the image positions and flux ratios are taken from Table 2 in Kochanek (1991). For 2237+0305, the image positions are taken from Rix, Schneider, & Bahcall (1992) while the flux ratios are taken from the C III] line observation by Racine (1992). For MG 0414+0453, the image positions and flux ratios are both from Katz & Hewitt (1993). We do not attempt to model 1422+231 as this system is more complex (see Kormann et al. 1994). Each of the four systems is modeled with $\beta = 0.5$, 1, and 1.5.

In Figure 1, we plot the resulting surface densities and external shears which are also listed in Table 1. Surprisingly, the values of κ and γ at the position of the images seem to be confined to a straight line for each β. With hindsight we were able to derive these loci from our model potential. The axis ratio R varies between 0.7 to 1 and depends linearly through equation (9) on the external shear γ_g. The range in γ_g or R is directly related to the range of κ or γ at the positions of the images (see eq. [5]). If we simply eliminate the

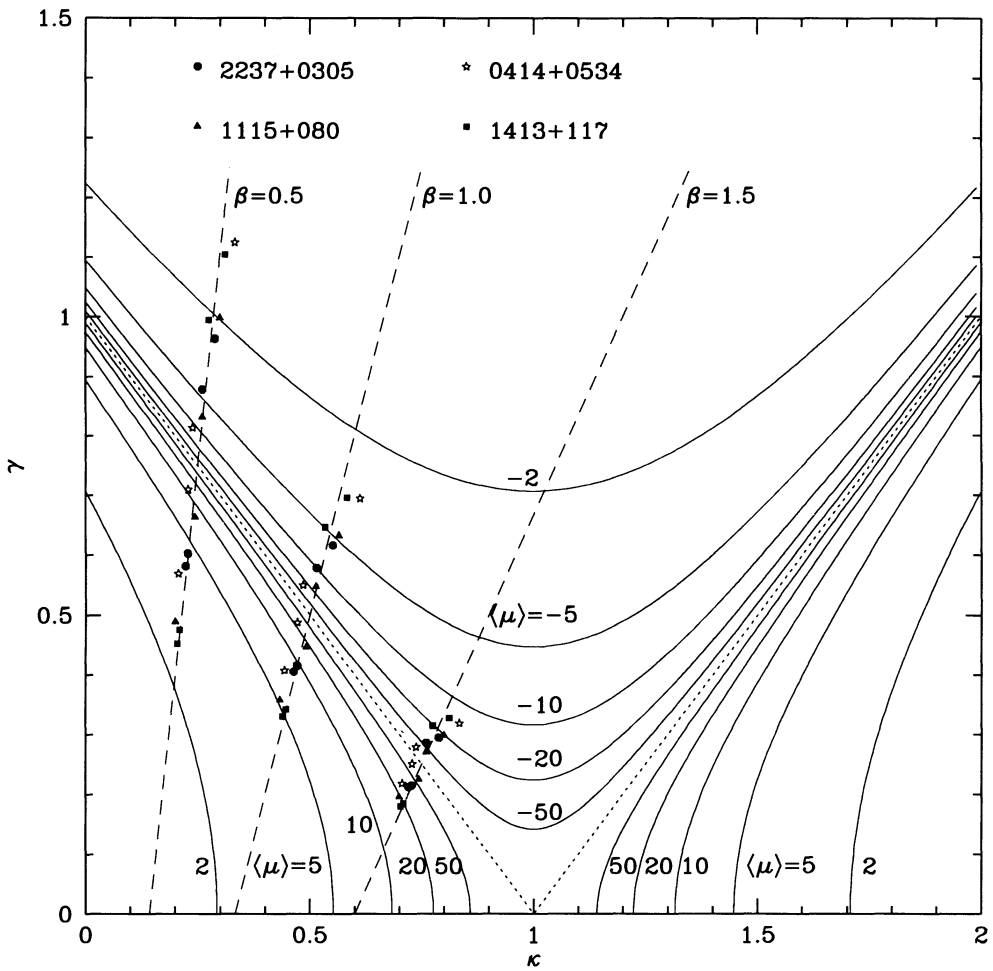

FIG. 1.—Surface densities (κ) and external shear (γ) are shown as different symbols for four quadruple lenses MG 0414+0534, PG 1115+080, 1413+117 and 2237+0305. All the systems are fitted with the simple galaxy potential model in eq. (1) with three different values of $\beta = 0.5$, 1, 1.5, 1422+231 is not shown because this system requires a much more complicated potential (see Kormann et al. 1994). The three dashed lines are the theoretical predictions for three β's (eq. [11]). The solid lines are isomagnification contours in the $\kappa - \gamma$ plane with the signs indicating the parities of magnification.

TABLE 1

SHEAR AND SURFACE DENSITY FOR THE IMAGES OF THE QUADRUPLE LENSES

	$\beta = 0.5$			$\beta = 1.0$			$\beta = 1.5$		
QSO	κ	γ	$\langle\mu\rangle$	κ	γ	$\langle\mu\rangle$	κ	γ	$\langle\mu\rangle$
2237+0305:									
A.....	0.228	0.603	4.3	0.471	0.416	9.4	0.728	0.215	36.5
B.....	0.223	0.582	3.8	0.464	0.406	8.1	0.723	0.212	31.3
C.....	0.289	0.964	−2.4	0.552	0.617	−5.6	0.789	0.296	−23.3
D.....	0.261	0.880	−4.4	0.515	0.579	−10.0	0.761	0.286	−40.7
1115+080:									
A_1.....	0.260	0.832	−6.9	0.514	0.548	−15.7	0.760	0.271	−63.6
A_2.....	0.244	0.664	7.7	0.492	0.447	17.2	0.744	0.226	68.3
B.....	0.300	0.999	−2.0	0.566	0.633	−4.7	0.800	0.300	−20.1
C.....	0.200	0.489	2.5	0.433	0.359	5.2	0.700	0.196	19.4
1413+117:									
A.....	0.275	0.995	−2.2	0.534	0.647	−5.0	0.775	0.315	−20.5
B.....	0.209	0.476	2.5	0.446	0.343	5.3	0.709	0.185	19.9
C.....	0.205	0.453	2.34	0.440	0.331	4.9	0.705	0.181	18.9
D.....	0.312	1.105	−1.3	0.583	0.697	−3.2	0.813	0.328	−13.8
0414+0534:									
A_1.....	0.229	0.710	11.1	0.472	0.488	24.2	0.729	0.251	94.4
A_2.....	0.239	0.814	−12.1	0.485	0.550	−26.8	0.738	0.279	−106.6
B.....	0.207	0.569	3.3	0.443	0.408	6.9	0.707	0.219	26.3
C.....	0.334	1.125	−1.2	0.613	0.695	−3.0	0.835	0.320	−13.3

NOTES.—Surface density κ and the shear γ at the position of the four macroimages for the four modeled quadruple lenses. $\langle\mu\rangle$ denotes the average magnification of the images. The sign indicates the parity of the image. β is the exponent in the potential and indicates a specific lens model with different slope (see eq. [1]).

global shear γ_g from equation (5) we obtain the following linear relationship of κ and γ at the position of the macroimages,

$$\gamma = \frac{4-\beta}{\beta}\kappa - 1 \tag{11}$$

The straight lines closely trace the points in the $\kappa - \gamma$-plane. Note that the spread of the points on the lines is larger for smaller β than for β close to 2 because of the factor $(2 - \beta)$ in equation (9).

The major uncertainty lies in the parameter β, which expresses the deviation of the potential from an isothermal sphere. There is little observational data on the mass distribution of elliptical galaxies although the rotation curves of spiral galaxies seem to indicate that the power law index lies in a narrow range $0.8 < \beta < 1.2$ for the bright galaxies (e.g., Persic & Salucci 1991). Furthermore, the observed lens sample is entirely consistent with $\beta = 1$ (Kochanek 1993), while other potential forms do not seem to be compatible with the observed sample (Maoz & Rix 1993). The allowed range of β may therefore be substantially narrower than the range plotted in Figure 1 ($0.5 < \beta < 1.5$), restricting the values of κ and γ to a smaller region than indicated.

3. MICROLENSING

In 2237+0305 microlensing is already well established. Based on the similarities of the surface densities and external shears between all the quadruple lenses, it is therefore natural to expect the probablility of microlensing to be roughly the same for all the quadruple lenses in Table 2. They would differ, however, in the timescale, magnitude, and frequency of microlensing. Their detectabilities for a given duration of observation will also vary. In what follows we briefly review the theory of microlensing, present some simple tools to estimate the microlensing activity for quadruple lenses and obtain a limit on the size of the source using the recent observations of MG 0414+0534.

3.1. *Theory of Microlensing*

From modeling the potential of a lensing galaxy, we obtain two essential microlensing ingredients. These are the surface mass density, κ, in units of the critical surface mass density and the external shear, γ, due to the surrounding matter at the macroimage. For a circular light bundle, the surface density only changes the size of the bundle while the external shear deforms the circular shape into an ellipse. These two parameters determine not only the average magnification of the image but also the global structure of the caustic network. In the following, we will assume all the mass is contained in compact objects like stars and ignore the smoothly distributed matter (see, e.g., Kayser & Refsdal 1989 for further discussion).

The timescale of microlensing, t_E is usually defined as the time taken by the source to cross one Einstein radius. It can be expressed as $t_E = \zeta_E/v_t$, where ζ_E is the projected Einstein radius on the source plane and v_t is the transverse velocity relative to the caustic network. ζ_E and its corresponding Einstein radius on the lens plane, z_E, are determined by the lens redshift, source redshift and the mass of the lens, M. The Einstein radius scales as $M^{1/2}$; therefore strictly speaking, the Einstein radius is a distribution determined by the stellar mass function. However, the influence of the stellar mass function can be mostly accounted for by its first moment—the average stellar mass (see, e.g., Witt, Kayser, & Refsdal 1993), $\langle M\rangle$. In most applications it is therefore appropriate to use identical lenses with mass equal to $\langle M\rangle$. We also adopt this approximation in our analysis.

TABLE 2

MICROLENSING PARAMETERS FOR QUADRUPLE LENSES

QSO	z_s	z_d	z_E (pc)	ζ_E (pc)	r_s/ζ_E	v_{MBR} (km s^{-1})	v_t (km s^{-1})	t_E (yr)	$\langle t_{HME}\rangle$ (yr)
2237+0305.....	1.695	0.0394	0.0016	0.013	0.013	58	3418	3.7	0.16
1115+080.....	1.72	0.29	0.0031	0.0049	0.033	94	496	9.7	1.1
1413+117.....	2.55	1.4*	0.0024	0.0021	0.077	280	155	13.3	3.6
0414+0534.....	2.63	0.468†	0.0034	0.0037	0.043	360	303	12.0	1.8
1422+231.....	3.62	0.64†	0.0035	0.0030	0.054	305	212	13.9	2.62

NOTES.—z_s is the redshift of the quasar and z_d is the redshift of the lensing galaxy. The asterisk (*) and dagger (†) denote the cases where the redshift of the lensing galaxy is assumed or not yet confirmed. z_E and ζ_E denote the Einstein radii in the deflector plane and the source plane, respectively, for an average stellar mass of $\langle M\rangle = 0.1\,M_\odot$ in the lensing galaxy. We assume a source radius $r_s = 0.5 \times 10^{15}$ cm. v_{MBR} denotes the transverse velocity of the observer relative to the microwave background radiation projected onto the line of sight to the quasar. v_t is the rms transverse velocity obtained by assuming the observer, lens and source each has a three-dimensional velocity of 400 km s^{-1} with their directions randomly distributed on the sky. $t_E = \zeta_E/v_t$ and $\langle t_{HME}\rangle$ is the expected average rise time of a microlensing event. A Friedmann cosmology with $\Omega = 1$, $\Lambda = 0$ and a Hubble constant of 75 km s^{-1} Mpc^{-1} are adopted.

The transverse velocity v_t can be obtained by summing the projected velocities of the observer, of the lensing galaxy and of the source at the source plane (Kayser et al. 1986). However, there is virtually no information about the velocities other than the velocity of the Galaxy relative to the microwave background. In Table 2, we give one estimate of the transverse velocity. We assume that each component (observer, lens and source) has a three-dimensional velocity of 400 km s^{-1} and their directions are random on the sky. The transverse velocity is then estimated as the rms of the velocity perpendicular to the line of sight by properly taking into account the geometrical and time dilation effects of the velocities (Kayser et al. 1986). We might also have obtained a different estimate of the transverse velocity by utilizing our projected transverse velocities v_{obs} relative to the microwave background in the direction of the quasars. We then assume that all the velocities are in the same direction and perpendicular to the line of sight with the lensing galaxies having a velocity of $v_d = 400$ km s^{-1} and that the quasars are static ($v_s = 0$). The transverse velocities derived in this way differ $\lesssim 25\%$ from the first estimates, and therefore are not shown in Table 2. We mention in passing that the frequency of microlensing is determined not only by the magnitude of the transverse velocity but also by the angle between the velocity and the external shear.

The most interesting events of the light curves are the high magnification events (HMEs), i.e., asymmetric peaks in the light curve (see Fig. 2*b*). They occur when the source crosses a microcaustic and two microimages (dis-)appear. The amplitude of HMEs (or general events) is determined not only by the microlensing parameters (or equivalently the caustic network) but also by the finite size of quasars. The finite size of a quasar provides an additional smoothing in the light curve, and is usually given in units of ζ_E. Loosely speaking, if the source radius is bigger than the average spacing between the caustics, then most (all) events are smeared out and only smooth and more symmetric-like variations can be observed (see Fig. 2*a* top panel). However, if the source radius is smaller than the typical spacing between the caustics, then most HMEs are resolved and are generally asymmetric. We can therefore roughly classify the light curves into two types, smooth and resolved, depending whether their source radius is larger or smaller than the average spacing between the caustics. For a resolved HME, the steep side of the peak is directly connected to the source size and the transverse velocity v_t. We will define the rise time of an event, t_{HME}, as the time interval between the bottom to the top of the event (see Witt & Mao 1994). The average rise time satisfies

$$\langle t_{HME}\rangle = c_{HME}\frac{r_s}{v_t}. \tag{12}$$

The constant c_{HME} depends on the source profile and also slightly on the direction of motion relative to the shear. For a source with Gaussian profile we obtain from numerical simulations $c_{HME} \approx 3.3$.[4]

We now consider the average spacing (time duration) between two caustics. The average spacing is obviously inversely proportional to the average number, $\langle N_{caustic}\rangle$, of caustic crossings (number of events) per unit length ζ_E or the corresponding time interval t_E. $N_{caustic}$ is independent of the average stellar mass and depends mainly on the average magnification $\langle\mu\rangle$ of the macroimage. For $\beta = 1$ we obtain along the line $\gamma = 3\kappa - 1$ in Figure 1 the following interpolation formulae from our numerical simulations:

$$\langle N_{caustic}\rangle_{\parallel} \approx 0.35\langle\mu\rangle = 0.35\frac{1}{4\kappa|1-2\kappa|} \quad \text{and} \quad \langle N_{caustic}\rangle_{\perp} \approx 0.7\frac{\sqrt{\kappa}}{2|1-2\kappa|} \tag{13}$$

The formula on the left side is for source motions parallel to shear and on the right side for motions perpendicular to the shear. While for source motions parallel to the shear the average number of caustic crossings increases in proportion to the magnification, we found that for motions perpendicular to the shear that the total number of caustic crossings for a whole track remains constant. Since the diameter of the total caustic network perpendicular to the shear is proportional to $|1-\kappa-\gamma|/\kappa^{1/2}$ (see, e.g., Kayser et al. 1986) we obtain the formula on the right side. In general $\langle N_{caustic}\rangle_{\perp} > \langle N_{caustic}\rangle_{\parallel}$.

[4] We assume here for the source profile $s(r) = (\sqrt{\pi}r_s)^{-1}\exp(-r^2/r_s^2)$. Note that in some papers the source radius is defined by $r_s = \sqrt{2}r_s'$.

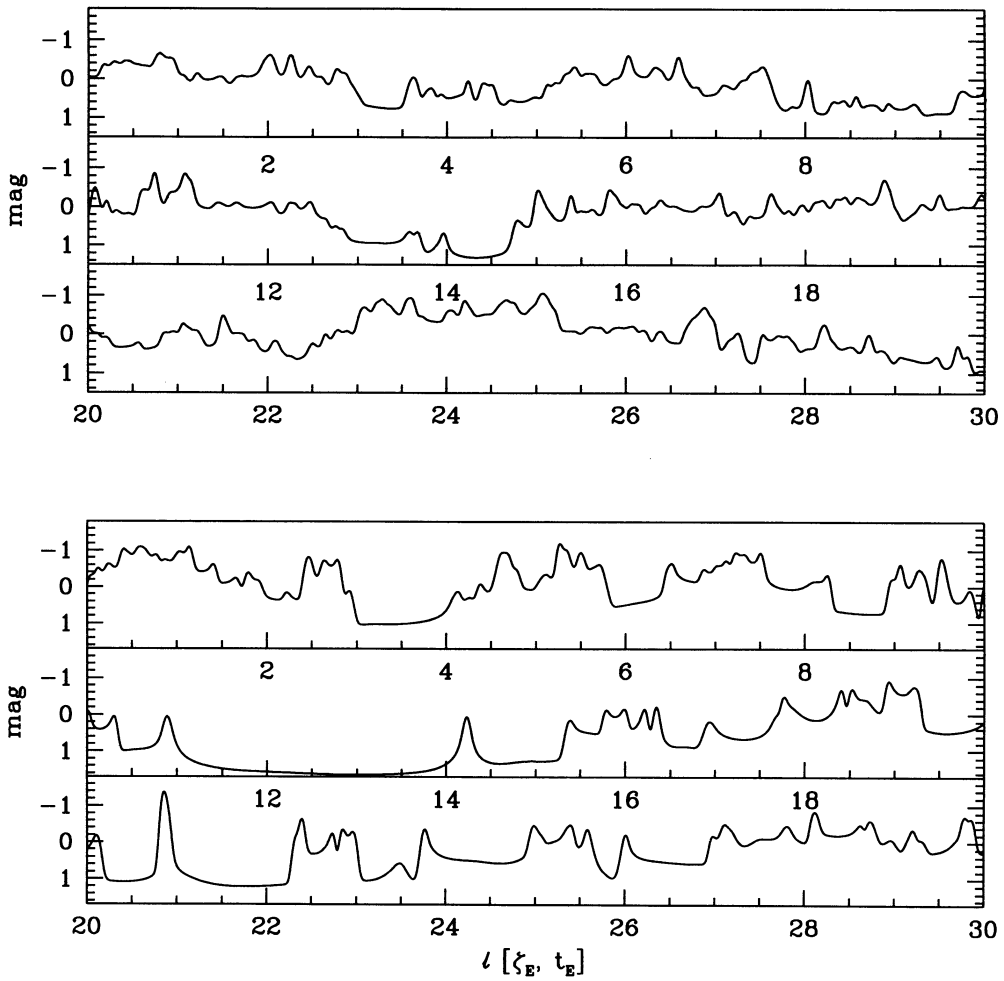

FIG. 2a

FIG. 2.—Three light curves for MG 0414+0534 for image A_1, B, and C perpendicular to the shear are shown. The light curve for image A2 is not shown because the pattern is similar to A_1. The macro parameters are adopted for the case $\beta = 1$ from Table 1. The quasar is assumed to have a Gaussian profile with a radius $r_s/\zeta_E = 0.04$. The light curves are obtained by convolving several parallel light curves for point sources with a Gaussian profile (see Witt 1994). The sample for the light curves contain 10^5–5×10^5 stars with equal mass. The horizontal axis is in units of the Einstein radius ζ_E or corresponding time unit t_E (see Table 1).

The duration of an event is approximately $2\langle t_{\rm HME}\rangle$. To obtain well resolved HMEs, the average duration of an event must be shorter than the average time interval between two adjacent caustics, i.e., $2\langle t_{\rm HME}\rangle = 2c_{\rm HME}\, r_s/v_t < t_E/\langle N_{\rm caustic}\rangle$. Thus the smaller the source "diameter" is compared with the spacing between the caustics the more likely it is to observe a single "clean" HME without any distortion. The rise time of a resolved HME event can be easily measured. In contrast, for $7r_s > \zeta_E/\langle N_{\rm caustic}\rangle$ the caustic network is too dense and almost no event can be identified. In particular, for $7r_s \gg \zeta_E/\langle N_{\rm caustic}\rangle$ we get only smooth, symmetric variations over a long timescale in the light curve. Using the values in Table 2 and equation (13) for $\beta = 1$, we find that the two quadruple quasars MG 0414+0534 and PG 1115+080 have the property that for images A_1 and A_2 the HMEs are smeared out (not resolved) while for the images B and C HMEs are less frequent and individually observable (see Fig. 2). The amplitude of events in B and C should be much stronger than in image A_1 and A_2. This is a promising circumstance, since after several years of observations it might be possible to classify the light curves for each image and therefore derive conclusions about the source size and the average stellar mass in the lensing galaxy. Since the Einstein radius in the source plane ζ_E is proportional to $\langle M\rangle^{1/2}$, we could for example exclude or confirm a hypothesis that the average stellar mass in the lensing galaxy is $\langle M\rangle = 10^{-5}\, M_\odot$ or smaller (see Refsdal & Stabell 1993). If the average mass is indeed so small, then no HMEs should be observable in any image and only smooth variations can occur.

3.2. *Optical Variability Caused by Microlensing in Quadruple Lenses*

The contribution of microlensing to the optical variability of quasars is still controversial. Generally speaking, if the variabilities are intrinsic, then high-redshift quasars should show less variability as they suffer more from time dilation. However, if microlensing contributed significantly to the variability, then the variability should not show a strong dependence on the redshift as the lenses are located at low redshift ($z \lesssim 1$) and the distances to the high-redshift ($z \gtrsim 2$) sources do not depend significantly on the redshift. Two recent studies have reached contradictory conclusions (Hawkins 1993; Hook et al. 1994, and references therein). We note that these

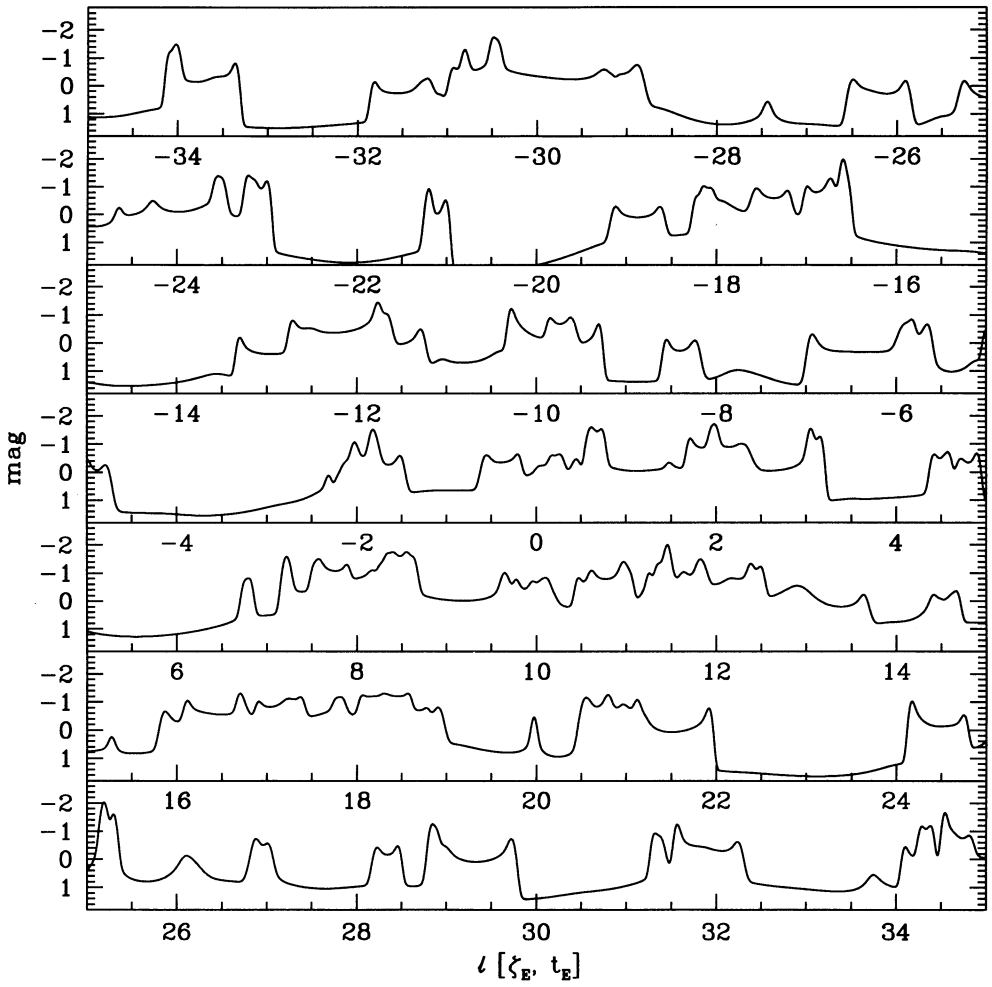

FIG. 2*b*

studies suffer the usual uncertainties induced by source evolution and potential observational biases. A definitive study must take these effects into consideration.

Despite the uncertainty in the role of microlensing for the variabilities in the general quasar population, we know microlensing must contribute to the variability in the quadruple quasars; therefore it is important to compute various measures of fluctuation in the light curve. We have computed the mean $\langle m \rangle$ and mean square brightness fluctuation $\langle \Delta m^2 \rangle^{1/2}$ (in magnitudes) caused by microlensing for very long light curves (800–1000 Einstein radii long), where

$$m(t) = -2.5 \log [\mu(t)/\langle \mu \rangle] , \qquad \text{and} \qquad \Delta m(t) = m(t) - \langle m(t) \rangle . \tag{14}$$

where $\langle \mu \rangle$ is the average magnification of the macroimage. In Figure 3 the results for $\langle m \rangle$ (*dashed lines*) and $\langle \Delta m^2 \rangle^{1/2}$ (*solid lines*) for the radii $r_s/\zeta_E = 0$, 0.1, and 1 is shown (*top to bottom*). The models are computed for the case $\beta = 1$ along the line $\gamma = 3\kappa - 1$ (see § 2). Each value was computed for three different samples of 10^5 stars with equal mass. In the top curve ($r_s = 0$) the error bars are indicated. While large experiments would give smaller uncertainties, the present experiments yield a number of interesting results.

We checked our results with the magnification fluctuations $\langle \mu^2 \rangle / \langle \mu \rangle^2$ obtained analytically by Seitz, Wambsganss, & Schneider (1994) for $r_s/\zeta_E = 0.01$ and 1.0 for $\gamma = 0$ and different densities κ. The values agree with each other within the error bars of our computations. The advantage of $\langle \Delta m^2 \rangle$ is that it converges even when $r_s \to 0$, whereas $\langle \mu^2 \rangle$ diverges to infinity as a result of the asymptotic behavior of magnification $p(\mu)d\mu \propto \mu^{-3} d\mu$, $\mu \to \infty$. The fluctuation for $r_s = 0$ is obviously an upper limit for the rms variability $\langle m_{\rm rms} \rangle = \langle \Delta m^2 \rangle^{1/2}$ caused by microlensing for an image of a (quadruple) quasar. We note that the quantity $\langle \Delta m \rangle$ cannot be determined directly by observations because of the unknown average magnification of the images; however the rms can be determined without the knowledge of the average magnification.

Examining Figure 3 we see that for images of positive parity the rms is about $\langle m_{\rm rms} \rangle \lesssim 0.6$ mag and for images of negative parity $\langle m_{\rm rms} \rangle \lesssim 0.9$ mag at a quadruple lens. The macroimages of positive parity have smaller fluctuations because their magnifications must be larger than one whereas the macroimages of negative parity have no lower limit in magnification. Thus for a given average magnification, the fluctuation for images with negative parity is larger. The rms becomes significantly smaller than the upper limits when $r_s/\zeta_E \gtrsim 1$, which might indicate (1) the source radius is very large, (2) the average stellar mass is quite small, or (3) the magnification of the image is very large with $\langle \mu \rangle \gtrsim 20$. Note that in Figure 3 as $\kappa \to 0.5$ the magnification becomes infinite and the

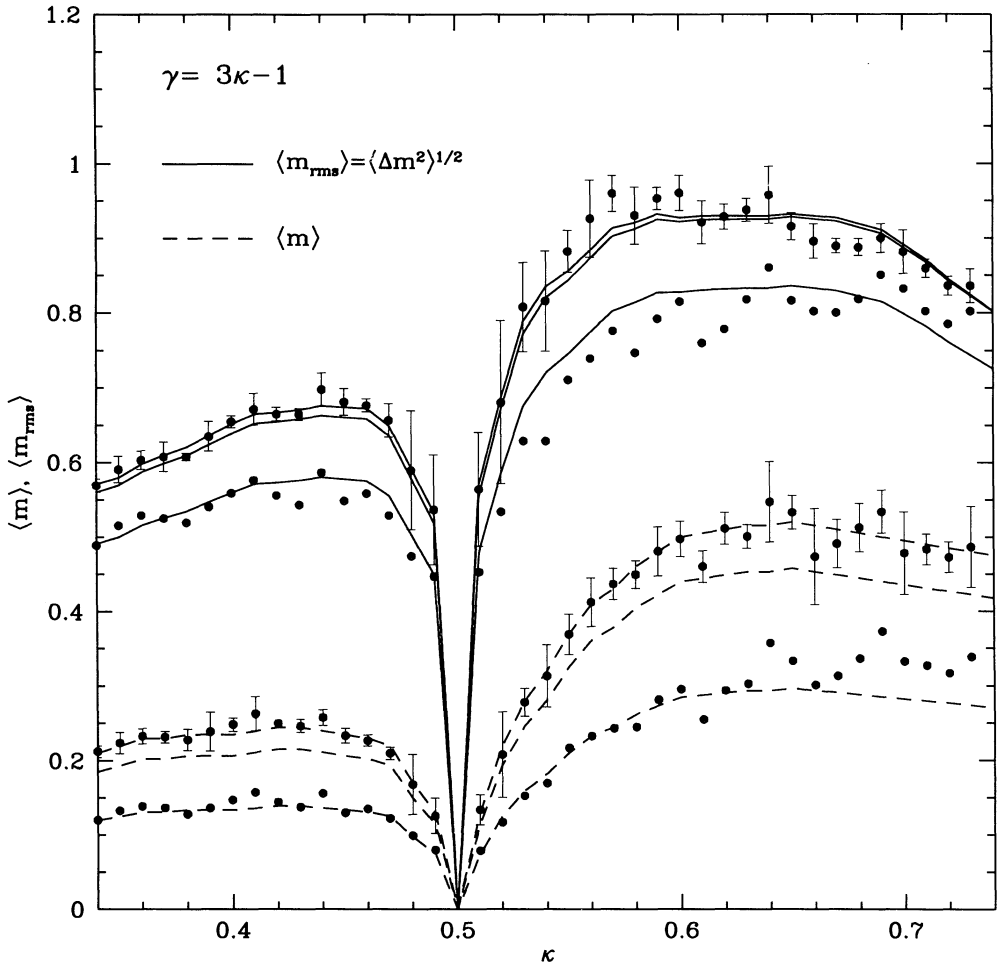

FIG. 3.—Mean $\langle m \rangle$ (*dashed lines*) and the rms $\langle m_{\rm rms} \rangle$ (*solid lines*) brightness fluctuation (in magnitude) are shown along the line of $\beta = 1$ as in Fig. 1. Three source radii, $r_s/\zeta_E = 0$, 0.1, 1.0 are shown (*from top to bottom*). Each value was computed for three different samples of 10^5 stars with equal mass. The error bars are only indicated for the case $r_s = 0$, but are similar for the other cases. For $r_s/\zeta_E = 0.1$ no dots are indicated and only the interpolated curves are shown. The interpolated curves are scaled by a constant factor to each other which leads to a slight mismatch to the computed values (*dots*) on the right side. Notice at $\kappa = \frac{1}{2}$ we have infinite magnification and the fluctuation is zero.

rms tends zero. We caution the observers that a small rms observed over a short period of time may not be interpreted in this way because the image can be in a quiescent state. Such a state can have magnitude variation smaller than 0.1 mag for $\approx 1 t_E$ (Witt & Mao 1994). Therefore reliable inferences can only be obtained when a lens has been observed for a sufficiently long time ($\gtrsim 3 t_E$).

3.3. *Microlensing in* MG 0414+0534?

Recent observations reported by Schechter & Moore (1993), Falco (1993), and Angonin-Willaime et al. (1994) in the *I*-band of the four images of MG 0414+0534 revealed some evidence that microlensing may be occurring in each of the four images. Each of the authors find significant differences between the observed radio flux ratios (see Hewitt et al. 1992 and Katz & Hewitt 1993) and the *I* band optical flux ratio. Schechter & Moore (1993) reported a flux ratio $A_2/A_1 = 0.45 \pm 0.06$ obtained from ground based data, which was subsequently confirmed with *HST* (Falco 1993) and CFHT (Angonin-Willaime et al. 1994). By contrast, in the radio, the flux ratio is $A_2/A_1 = 0.9$ (Katz & Hewitt 1993), close to the theoretically expected value. The predicted near equality of A_1 and A_2 results from their lying close to a critical curve. The optical to radio flux ratios for components B and C agree more closely with component A_1 than with A_2.

It might be that the quasar is varying intrinsically, with the difference in the flux ratio due to the time delay between inages. Since this would mean that the source is varying by more than a factor of 2 on the scale of the time delay (less than a few hours), we regard this as unlikely. A more natural explanation is microlensing. It is believed that the source size of a quasar in the radio band is at least one hundred times larger than that in the optical continuum (Blandford 1990). We therefore expect little or no effect due to microlensing in the radio band but significant effects in the optical band. This would provide us with a very plausible explanation for the observed flux ratio differences in the *I* and radio bands. For the sake of argument we would then assume that the observed flux ratio in the optical is due to microlensing and derive an upper limit for the source radius under this assumption.

In Figure 4 we show the computed flux ratio of the images A_2/A_1 for three different source radii $r_s/\zeta_E = 0.04$, 0.1, and 1.0. We took $\beta = 1$ for the macromodel as reported in Table 1. The theoretical flux ratio of our model is $A_2/A_1 = 1.1$, differing somewhat from the

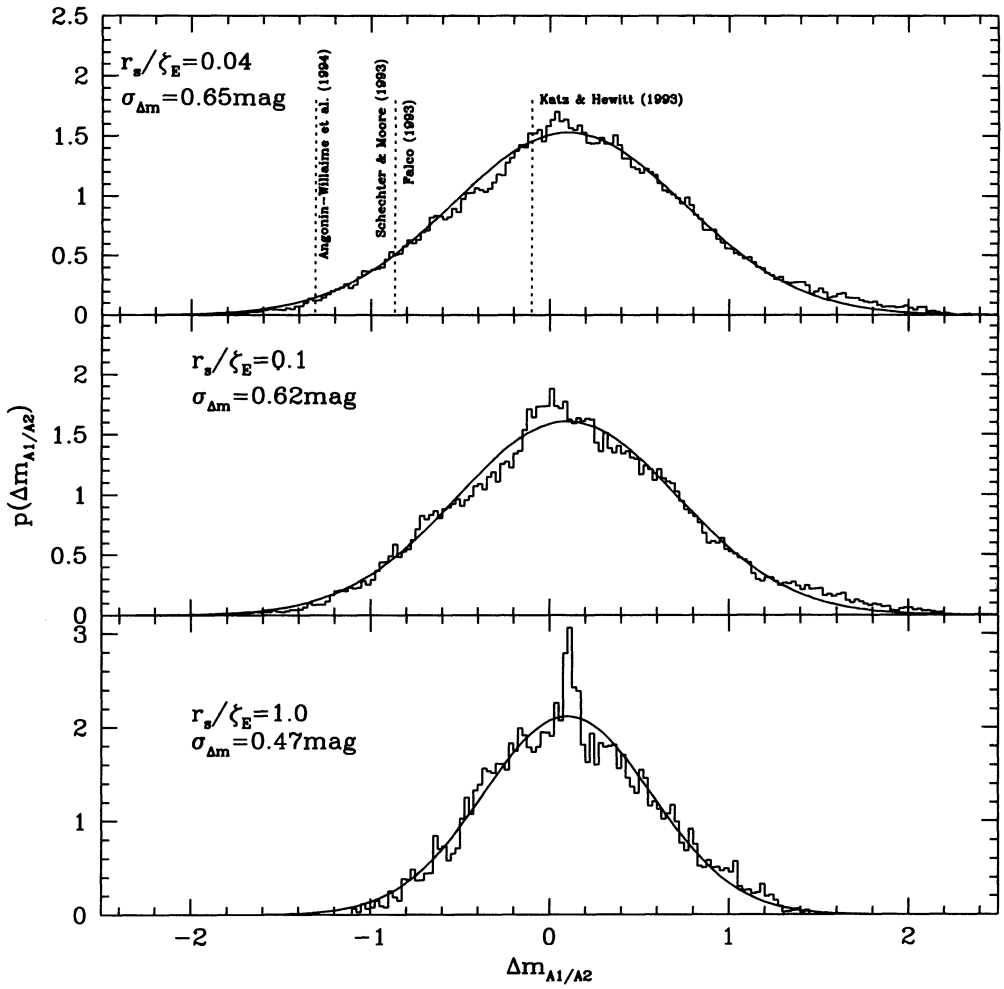

FIG. 4.—Probability distributions of the flux ratio for the bright image pair A_1/A_2 of MG 0414+0534 for three source radii, r_s/ζ_E = 0.04, 0.1, 1.0. The solid line indicates the best fit of eq. (15) of a Gaussian profile. The standard deviation of the flux ratio $\sigma_{\Delta m}$ is indicated for each panel. Error bars are not indicated. Notice when the source radius increases, the distribution narrows and converges to the mean flux ratio and therefore increasingly unlikely to have the observed flux ratio.

observed ratio in the radio. Such disagreement is common in the modeling and probably indicates oversimplification in the parameterization of the potential. However, this uncertainty does not change our results significantly. The light curves are computed for a sample of 5×10^5 stars of equal mass perpendicular to the shear. A Gaussian source profile was adopted (for method see Witt 1993, 1995). In Figures 2*a* and 5 the light curves of image A_1 are shown for three different source radii. The computed distribution of the magnitude difference of image A_1 and A_2 can be fitted well by a Gaussian distribution (*solid line*, Fig. 4)

$$p(\Delta m_{A_1/A_2}) = \frac{1}{\sqrt{2\pi}\sigma_{\Delta m}} \exp\left[-\frac{(\Delta m_{A_1/A_2} - 0.1)^2}{2\sigma_{\Delta m}^2}\right]. \tag{15}$$

with

$$\Delta m_{A_1/A_2} = m_{A_1} - m_{A_2} = 2.5 \log \frac{A_2}{A_1}, \tag{16}$$

where $\sigma_{\Delta m}$ is the standard deviation of the distribution in magnitudes. The distribution is slightly shifted because the theoretical average flux ratio is $A_2/A_1 = 1.1$ equivalent to 0.1 mag. The Gaussian shape of the distributions is the natural result of the central limit theorem. The flux ratio distribution becomes narrower ($\sigma_{\Delta m}$ decreases) for larger source radii. Thus the observed optical flux ratio for A_2/A_1 is unlikely, but not ridiculously so if the source is small. An estimate of the probability to observe the optical flux ratio for MG 0414+0543 yields $P(0.4 < A_1/A_2 < 2.5) = P(-1 < \Delta m_{A_1/A_2} < 1) = 0.87$ for $r_s/\zeta_E = 0.04$ and 0.96 for $r_s/\zeta_E = 1.0$.

From the standard deviations for three different source radii (r_s/ζ_E = 0.04, 0.1, and 1.0), we can obtain an approximate scaling formula between these two quantities ($\sigma_{\Delta m}$ and r_s)

$$\frac{1/\sigma_{\Delta m1} - 1/\sigma_{\Delta m,\max}}{1/\sigma_{\Delta m2} - 1/\sigma_{\Delta m,\max}} \approx \left(\frac{r_1}{r_2}\right)^{1/2} \tag{17}$$

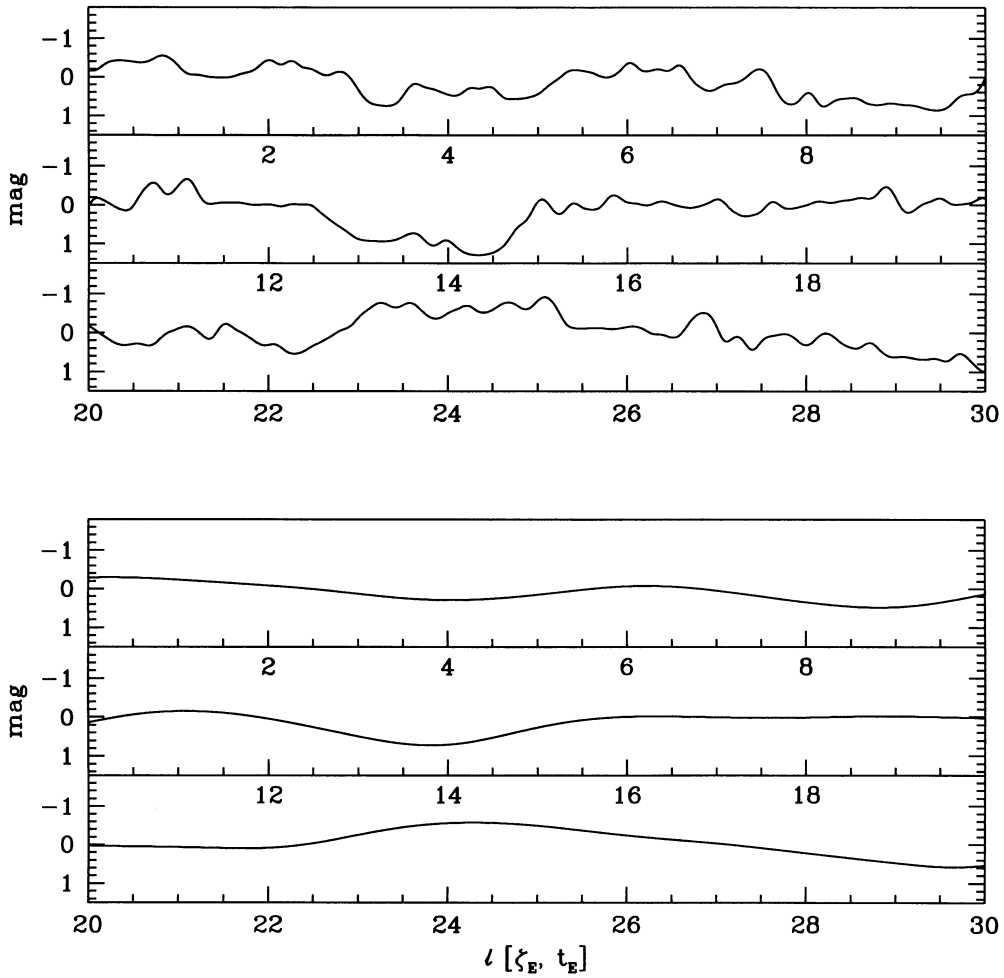

FIG. 5.—Two light curves for MG 0414+0534 for image A_1 perpendicular to the shear are shown. The macro parameter are adopted for the case $\beta = 1$ in Table 1. The radius of the source is $r_s/\zeta_E = 0.1$ (*top*) and 1.0 (*bottom*). 5×10^5 stars were used to compute the light curves. The notations are the same as in Fig. 2.

where r_1 and r_2 are two source radii, and $\sigma_{\Delta m1}$ and $\sigma_{\Delta m2}$ are their corresponding standard deviations and $\sigma_{\Delta m,\max} \approx 0.72$ mag in this case. $\sigma_{\Delta m,\max}$ is the maximum standard deviation which is obtained in the limit of an unresolved source ($r_s = 0$). We note that the standard deviation does not diverge to infinity for $r_s \to 0$ because of the finite limit of the rms as obtained in § 3.2. We also caution that the scaling formula may not be valid for large sources (see Refsdal & Stabell 1993 for an analytical formula for $\gamma = 0$), although it gives the correct asymptotic behavior ($\sigma_{\Delta m} \to 0$ when $r_s \to \infty$). Considering this limit of the standard deviation it is somewhat unusual that one observed a difference of $\Delta m_{A_1/A_2} = -1$ mag in the two images A_1 and A_2. This observation is, however, not outside the 2 σ limit. If the microlensing interpretation is correct we expect that $\Delta m_{A_1/A_2}$ will increase in the coming years. However, if the flux ratio remains constant, this will favor the argument that we observe differential reddening (Lawrence et al. 1995) or magnification gradients in the two components.

Assuming that the flux discrepancy is due to microlensing, we can use equation (17) to set limits on the source radius for any given observed flux ratio. For MG 0414+0534, we obtain a 95% limit for $P(0.4 < A_1/A_2 < 2.5) = 0.95$ when $r_s/\zeta_E \approx 0.92$. In other words, the 95% limit of the source radius in the optical is $r_s \lesssim 0.92\zeta_E \approx 10^{16}(\langle M \rangle/0.1\ M_\odot)^{1/2}$ cm. Examining the light curves in Figures 2 and 5 for image A_1 and different source radii reveals very different timescales for the microlensing variations which we did not consider in our analysis. A tighter limit on the source radius is possible with more observations and more thorough analysis of other information contained in the light curves.

4. DISCUSSION

We have shown that the configuration of image positions of almost every known quadruple lens can be reproduced by a simple potential model with a variable power law slope. The assumed slope of the lensing galaxy is closely coupled to the magnification of the images. Shallow slopes for the surface mass density of the lensing galaxy give higher magnifications than steeper slopes. For this reason a King model or a de Vaucouleurs model for a galaxy would predict smaller magnification for the images of a quadruple lens than an isothermal sphere model. To avoid this ambiguity and a biasing of the results it is important to find models (ideally nonparametric) which can actually fit all the observed data including the flux ratios of the images. Another way to distangle information about the potential shape of the lensing galaxy is to combine observations of microlensing with the models of the

potential. Throughout the paper, we have assumed that the smoothly distributed matter is not important, it is not clear whether this assumption is valid as the nature of dark matter is still an open question. If the contribution of the smoothly distributed matter is not negligible, then the microlensing parameters of quadruple lenses have to be modified (Kayser & Refsdal 1989). The ongoing experiments to detect massive compact objects in the Galactic halo should shed some light on this problem (Aubourg 1993; Alcock et al. 1995; Udalski et al. 1994, and references therein).

We have obtained from the numerical simulations the average spacing between caustics. Based on this knowledge, we present a simple criterion to classify the light curves into two categories, smooth and resolved, depending on the relative sizes of the source radius and the average spacing between caustics. We propose to use the rms of the *magnitude* to measure fluctuations in the light curve because $\langle \mu^2 \rangle$ diverges for a point source. Using this statistic we obtained, for the first time, an upper limit for the rms variability caused by microlensing in quadruple lenses. For MG 0414+0534 an upper limit for the source radius is obtained, assuming the differences of the observed flux ratios in radio and optical band in image A_1 and A_2 are due to microlensing. This is possible because the close pair A_1 and A_2 are predicted to have a flux ratio very close to 1. This method fails currently to yield limits for PG 1115+080 because the observed flux ratio in the optical is close to the theoretical predicted one.

For all the quadruple lenses, microlensing seems inevitable. For MG 0414+0534 and PG 1115+080, there is already observational evidence for microlensing. Regular samplings of these systems would allow a systematic analysis of their light curves. To resolve HMEs in the light curve, we recommend that the frequency of observation should be every $\langle t_{\rm HME} \rangle/10$ days for the quadruple lenses. This would mean 2237+0305, MG 0414+0534, and PG 1115+080 would be observed roughly every 10 days, 50 days and 40 days, respectively. Besides such regular observations, one would benefit from observing every day for one to two weeks during a year to rule out any intrinsic variability of the quasar. If a quasar has intrinsic variability then the frequency of observations has to be adjusted to this timescale as well in order to discriminate between microlensing and intrinsic variability.

We are grateful to Bohdan Paczyński for useful discussions and criticisms and we also would like to thank Carolin Seitz for providing us with some data about the magnification fluctuation. We also thank Rolf Stabell and an anonymous referee for constructive comments. This work was supported by NASA grant NAGW-2448, by NSF grants AST 90-23775 and AST 93-13620, and in part by a research fellowship of the Deutsche Forschungsgemeinschaft (DFG) under Az. Wi 1122/1-1.

REFERENCES

Alcock, C., et al. 1995, ApJ, submitted
Altieri, B., & Giraud, E. 1991, ESO Messenger, 63, 65
Angonin-Willaime, M. C., Vanderiest, C., Hammer, F., & Magain, P. 1994, A&A, 281, 388
Arnould, P. et al. 1993, in Proc. 31st Liège International Colloq., ed. J. Surdej et al. (Liège: Univ. Liège), 169
Aubourg, E., et al. 1993, Nature, 365, 623
Blandford, R. D. 1990, in Active Galactic Nuclei, ed. R. Blandford, H. Netzer, & L. Woltjer (Berlin: Springer), 258
Blandford, R. D., & Narayan, R. 1992, ARA&A, 30, 311
Chang, K., & Refsdal, S. 1979, Nature, 282, 561
Falco, E. E. 1993, in Proc. 31st Liège International Colloq., ed. J. Surdej et al. (Liège: Univ. Liège), 127
Falco, E. E., Wambsganss, J., & Schneider, P. 1991, MNRAS, 251, 698
Gott, J. R. 1981, ApJ, 243, 140
Hawkins, M. R. S. 1993, Nature, 366, 242
Hewitt, J. N., Turner, E. L., Lawrence, C. R., Schneider, D. P., & Brody, J. P. 1992, AJ, 104, 968
Hogg, D. W., & Blandford, R. D. 1994, MNRAS, 268, 889
Hook, I. M., McMahon, R. G., Boyle, B. J., & Irwin, M. J. 1994, MNRAS, 268, 305
Houde, M., & Racine, R. 1994, AJ, 107, 466
Irwin, M. J., Webster, R. L., Hewett, P. C., Corrigan, R. T., & Jedrzejewski, R. I. 1989, AJ, 98, 1989
Katz, C. A., & Hewitt, J. N. 1993, ApJ, 409, L9
Kayser, R., & Refsdal, S. 1989, Nature, 388, 745
Kayser, R., Refsdal, S., & Stabell, R. 1986, A&A, 166, 36
Kayser, R., Surdej, J., Condon, J. J., Hazard, C., Kellermann, K. I., Magain, P., Remy, M., & Smette, A. 1990, ApJ, 364, 15
Kochanek, C. S. 1991, ApJ, 373, 354
———. 1993, ApJ, 419, 12
Kormann, R., Schneider, P., & Bartelmann, M. 1994, A&A, 286, 357
Lawrence, C. R., Cohen, J. G., & Oke, J. B. 1995, AJ, submitted
Maoz, D., & Rix, H.-W. 1993, ApJ, 416, 425
Pen, U.-L., et al. 1993, in Proc. 31st Liège International Colloq., ed. J. Surdej et al. (Liège: Univ. Liège), 111
Persic, M., & Salucci, P. 1991, ApJ, 368, 60
Racine, R. 1992, ApJ, 395, L65
Refsdal, S., & Surdej, J. 1994, Rep. Progr. Phys., 57, 117
Rix, H. W., Schneider, D. P., & Bahcall, J. N. 1992, AJ, 104, 959
Schechter, P. L. 1995, in preparation
Schechter, P. L., & Moore, C. B. 1993, AJ, 105, 1
Schild, R. E., & Smith, R. C. 1991, AJ, 101, 813
Schneider, P., Ehlers, J., & Falco, E. E. 1992, Gravitational Lenses (Berlin: Springer)
Seitz, C., Wambsganss, J., & Schneider, P. 1995, A&A, submitted
Surdej, J., Fraipont-Caro, D., Gosset, E., Refsdal, S., & Remy, M. eds. 1993, Proc. 31st Liège International Colloq. (Liège: Univ. Liège)
Udalski, A., Szymański, M., Mao, S., DiStefano, R. I., Kałużny, J., Kubiak, M., Mateo, M., & Krzemiński, W. 1994, ApJ, 436, 103
Vanderiest, C., et al. 1986, A&A, 158, L5
Wambsganss, J., & Paczyński, B. 1991, AJ, 102, 864
———. 1995, AJ, in press
Witt, H. J. 1993, ApJ, 403, 530
———. 1995, in preparation
Witt, H. J., Kayser, R., & Refsdal, S. 1993, A&A, 268, 501
Witt, H. J., & Mao, S. 1994, ApJ, 429, 66
Young, P. 1981, ApJ, 244, 756